RSC Advances

ROYAL SOCIETY OF CHEMISTRY

PAPER

View Article Online
View Journal | View Issue

Cite this: *RSC Adv.*, 2022, **12**, 12891

Controlled synthesis of trimetallic nitrogen-incorporated CoNiFe layered double hydroxide electrocatalysts for boosting the oxygen evolution reaction†

Anh Thi Nguyet Nguyen, Minji Kim and Jun Ho Shim *

Received 12th February 2022
Accepted 20th April 2022

DOI: 10.1039/d2ra00919f

rsc.li/rsc-advances

The development of non-precious trimetallic electrocatalysts exhibiting high activity and stability is a promising strategy for fabricating efficient electrocatalysts for the oxygen evolution reaction (OER). In this study, trimetallic nitrogen-incorporated CoNiFe (N–CoNiFe) was produced to solve the low OER efficiency using a facile co-precipitation method in the presence of ethanolamine (EA) ligands. A series of CoNiFe catalysts at different EA concentrations were also investigated to determine the effects of the ligand in the co-precipitation of a trimetallic system. The introduction of an optimized EA concentration (20 mM) improved the electrocatalytic performance of N–CoNiFe dramatically, with an overpotential of 318 mV at 10 mA cm^{-2} in 1.0 M KOH and a Tafel slope of 72.2 mV dec^{-1}. In addition, N–CoNiFe shows high durability in the OER process with little change in the overpotential (*ca.* 16.0 mV) at 10 mA cm^{-2} after 2000 cycles, which was smaller than that for commercial Ir/C (38.0 mV).

Introduction

Hydrogen is a promising clean fuel and an important part of the future of renewable energy in addressing the global energy demand and environmental issues.[1] Despite this, one of the major problems in the hydrogen economy is its clean production because most of the hydrogen currently used is produced from fossil fuel *via* the steam reforming process, with carbon dioxide as a byproduct.[2] Therefore, considerable effort has been made to produce hydrogen from water electrolysis, which is an environmentally clean, potentially cost-effective, and renewable source of hydrogen.[3] Water electrolysis consists of two half-cell reactions, the hydrogen evolution reaction (HER) at the cathode and the oxygen evolution reaction (OER) at the anode. For the reaction to proceed, electrochemical water splitting theoretically requires a high potential of 1.23 V between the anode and cathode because of the four-electron transfer in the OER mechanism.[4] The sluggish kinetics leads to lower efficiencies for water splitting. Accordingly, a highly efficient electrocatalyst is needed to decrease the overpotential as much as possible.

Currently, noble metals and noble metal-based oxides (especially Ru, Ir, and their oxides)[5,6] are considered the most effective electrocatalysts for water splitting, but they are unavailable for large-scale application owing to their high cost and low natural abundance.[4] Over the past decades, tremendous progress has been made in transition metal-based electrocatalysts, such as metal oxide,[7,8] metal phosphide,[9] and metal chalcogenides.[10] These catalysts can be promising alternative materials with good OER performances for electrochemical water splitting. Moreover, the interactions between the various compositions in a multi-metallic structure can produce additional synergistic effects, optimize the adsorption energies, or increase the electrical conductivity compared to monometallic derivatives.[11] For example, Kuai *et al.* prepared a broader range of amorphous Fe–Ni–O(x) using an aerosol-spray-assisted approach.[12] Fe–Ni mixed oxides exhibited better OER activity than pure Fe or Ni oxides because of the synergistic effect between different metal sites. In particular, the $Fe_6Ni_{10}O_x$ composition showed an overpotential of as low as 0.286 V (*vs.* RHE) at 10 mA cm^{-2} and a Tafel slope of 48 mV dec^{-1}. Yang *et al.* reported that increasing the Fe and Ni concentrations in Co-MOF produced different catalytic efficiencies.[13] The bimetallic CoFe-MOF prepared hydrothermally showed better OER performance with an overpotential of 0.355 V (*vs.* RHE) at 10 mA cm^{-2} in 0.1 M KOH and a decent Tafel slope of 49 mV dec^{-1}, which is better than the monometallic Co-MOF. On the other hand, we demonstrated that CoFe nanocubes with tunable porosity could significantly increase the OER and ORR activity in a previous investigation.[14] The CoFe composition in microporous catalysts (average pore diameter, $d \leq 2$ nm) had a larger effect on the OER than the ORR, whereas microporous/mesoporous structures ($d \approx 35.6$ nm) favored the ORR catalytic activity.[14] Smith *et al.* extended the combination of

Department of Chemistry and Institute of Basic Science, Daegu University, Gyeongsan 38453, Republic of Korea. E-mail: junhoshim@daegu.ac.kr

† Electronic supplementary information (ESI) available. See https://doi.org/10.1039/d2ra00919f

trimetallic Ni–Co–Fe system, in which the Fe concentration was maintained at 20–40% and the onset potential and Tafel slope were the lowest, regardless of whether the other metal component was Ni or Co.[15]

Recently, transition metal-based layered double hydroxides (LDHs) have attracted considerable attention in water oxidation because of many advantages, such as rich active site comparison with the 0D and 1D materials, large surface area, excellent structural and compositional tunability, strong electrostatic interactions between layers and interlayers anions, hierarchical porosity accelerating the diffusion of water molecules and release of gaseous products, and their promising electrocatalytic performance.[16] Among various LDHs systems, such as NiFe,[17] NiMn,[8] NiCo,[18] and CoFe,[19] NiFe LDH or NiFe (oxy) hydroxides are the most active OER catalyst compared to other bimetallic LDHs under alkaline conditions.[17] On the other hand, the effect of promoting cooperation between different metal ions in this OER catalyst may not be limited to Ni and Fe metals. A recent study reported that the addition of a third metal (*e.g.*, Co, Cr, Mn, or Mo) could further improve the catalytic activity.[20–22] Qu *et al.* synthesized CoNiFe-LDH nanocage with cation exchange reaction using a metal–organic framework as a template, which exhibited a low overpotential of 299 mV (10 mA cm^{-2}, 1 M KOH) with a Tafel slope of 50 mV dec^{-1}.[21] Jin *et al.* reported that the trimetallic properties of Ni, Fe, and Cr provide opportunities to generate strong electron interactions within the metal hydroxide matrix and enhance the synergy between metals toward the OER.[22] The introduction of multivalent Cr ion into NiFe can readily adopt various oxidation states during the OER reactions, indicating a positive effect on active species for water oxidation.[22] Although the identity of the catalytic active sites remains unclear, a third metal introduction and its positive influence on the local electronic structure produces a favorable OER process.

Incorporating a heteroatom into a metallic compound was a practical approach to modify the electronic structure to boost the intrinsic activity of electrocatalysts.[23–28] For example, sulfur-doped cobalt,[25] nitrogen-doped cobalt oxide,[26] sulfur-doped NiCoFe LDH nanosheet,[27] and phosphorus-doped Ni_3S_2/$CoFe_2O_4$ arrays on nickel foam[28] exhibited significantly enhanced electrocatalytic performance toward OER. Lu *et al.* revealed a facile and practical pathway for hierarchical fabrication of 3D porous S-incorporated NiCoFe LDH nanosheets on carbon cloth.[27] S doping increases the electrical conductivity of LDH, and the high catalytic efficiency for the OER was attributed to the enhancement of substantial active sites on the surface of S–NiCoFe LDH.[27] Joo *et al.* suggested that the addition of gaseous boronization into NiFe-LDH enhances the OER electrocatalytic activity.[29] This strategy increases the oxyhydroxides ratio of LDHs, which has a positive effect on the OER performance.[29] On the other hand, because of the poor electrical conductivity of the LDHs, carbon materials, including graphene oxide (GO) and carbon nanotubes, doped with heteroatoms, such as B, N, S, and P have been demonstrated to be electrochemically active. Sun *et al.* prepared vertically aligned ternary NiCoFe-LDHs on defect-rich and N-doped crumpled GO by *in situ* routes.[30] Owing to the synergistic effect between NiCoFe-LDH and N–GO, the prepared composite contained a larger number of active sites and fast electron transfer as an efficient bifunctional catalyst for OER/ORR.[30]

This paper reports a trimetallic nitrogen-incorporated CoNiFe LDHs (N–CoNiFe) fabricated using a rapid, inexpensive, and facile co-precipitation method in the presence of ethanolamine (EA). The enhanced OER performance was attributed to the following reasons: (1) synergistic effect between the different metal sites; (2) fully and uniformly exposed active sites in the two-dimensional sheets; (3) LDHs structure allows the intercalation of water molecules and anions, provide better bulk redox activity; (4) successful incorporation of the nitrogen element into the CoNiFe boosts the OER activity of N–CoNiFe considerably by enhancing its electrical conductivity and tuning the energy barrier for the adsorption of OER intermediates on the catalyst surface.

Experimental

Chemicals

Cobalt(II) acetate tetrahydrate ($Co(Ac)_2 \cdot 4H_2O$), iron(III) chloride ($FeCl_3$), and ethanolamine (EA) were purchased from Sigma-Aldrich. Nickel(II) chloride hexahydrate ($NiCl_2 \cdot 6H_2O$) was obtained from Duksan Co. (Korea). E-TEK supplied the commercial Ir/C catalysts (20 wt% loading) and Vulcan XC-71 as the supporting material. The aqueous solutions were prepared using deionized water. All other chemicals were used as received.

Synthesis of trimetallic nitrogen-incorporated CoNiFe LDHs

Briefly, $Co(Ac)_2 \cdot 4H_2O$, $NiCl_2 \cdot 6H_2O$, and $FeCl_3$ ($[Co^{2+}] : [Ni^{2+}] : [Fe^{3+}] = 1 : 2 : 1$ molar ratio) were dissolved in 15 mL of H_2O in a 100 mL three-neck flask. Subsequently, 2 mL of EA was added dropwise with magnetic stirring and heated to 100 °C for 2 h. The catalyst suspension was heated on a heating mantle equipped with a reflux condenser to maintain the temperature and solvent volume during the reaction. After cooling to room temperature, the precipitated gel was collected by centrifugation, washed once with deionized water, and freeze-dried to obtain trimetallic N–CoNiFe LDHs. The resulting powder product was calcined at 200 °C with a heating rate of 5 °C min^{-1} and maintained for 1 h under a N_2 atmosphere. Combinations of monometallic and bimetallic catalysts were prepared using the same method and denoted as N–Co, N–Ni, N–Fe, N–NiFe, N–CoNi, and N–CoFe catalysts, respectively. N-free CoNiFe synthesized without EA was also prepared to compare the effect of nitrogen incorporation on the electrocatalytic activity.

Characterization

The morphologies of all samples were observed by high-resolution transmission electron microscopy (HR-TEM, Philip, CM-200) and scanning electron microscopy (SEM, S-4800) equipped with EDS (energy-dispersive X-ray spectroscopy). Powder X-ray diffraction (XRD, Rigaku D/max-2500) was performed using Cu Kα radiation (λ = 1.54 Å). The surface

properties of the catalysts were examined by X-ray photoelectron spectroscopy (XPS, AXIS Nova) using Al Kα monochromatized radiation. The Brunauer–Emmett–Teller (BET) surface area and pore size distributions of catalysts were analyzed using a BELSORP-mini II (Mictrotrac-BEL, Japan).

Electrochemical measurements

All electrochemical experiments were carried out in a three-electrode system using mercury–mercury oxide (Hg/HgO), Pt wire, and glassy carbon (GC) as the reference, counter, and working electrodes, respectively, on a rotating disk electrode (RDE, BAS Bioanalytical System). Typically, each prepared catalyst was mixed with the supporting carbon material (1 : 1 weight ratio) and dispersed ultrasonically in water for 30 min (2.0 mg mL^{-1}). Subsequently, 15 μL of catalyst ink was dropped onto a GC electrode (3 mm diameter, 0.42 mg cm^{-2}) and dried at room temperature under vacuum. The electrode was covered with 5 μL of 0.5 wt% Nafion. For comparison, Ir/C was prepared using the same method. All electrochemical measurements were performed at a scan rate of 10 mV s^{-1} in aqueous O_2-saturated 1.0 M KOH solutions. All potentials presented in this study are referenced to the reversible hydrogen electrode (RHE) according to the Nernst equation. To determine the electrochemical surface area (ECSA), cyclic voltammetry (CV) was conducted over the potential range of 0.92 to 1.02 V (*vs.* RHE), which is located at the non-faradaic region to explore the electrochemical double-layer capacitance (C_{dl}). Electrochemical impedance spectroscopy (EIS) was performed at $\eta = 337.4$ mV (*vs.* RHE) in a frequency range over 0.1 Hz to 100 kHz by applying an AC voltage of 5 mV amplitude. For the OER measurements, linear sweep voltammetry (LSV) was conducted by sweeping the potential from 1.22 V to 1.82 V (*vs.* RHE) at a scan rate of 10 mV s^{-1} and a fixed rotation rate of 1600 rpm.

Results and discussion

Morphological and structural characterization

Fig. 1 presents the facile and one-step synthesis of trimetallic N–CoNiFe LDHs electrocatalysts by precipitation. The as-prepared complexes were formed between the transition metals (Co, Ni, and Fe) and EA at high temperatures *via* dative covalent bonds, in which both electrons originate from the amino ($-NH_2$) and hydroxyl (–OH) groups. EA plays a crucial role as a ligand for fabricating metal hydroxide $M(OH)_x$, the nucleophilicity of the donor atoms, stabilizing agent, and a nitrogen/oxygen source that can tune the electronic, solubility, and steric properties of the catalytic systems.[31–33] Finally, calcination at 200 °C for 1 h under a N_2 atmosphere helps to stabilize the structure of the metal-based LDHs.

The morphology of the prepared catalysts was examined by SEM. Flower-shaped particles were observed in N–Co (Fig. S1a†) with a particle diameter of 1–3 μm. Nanoflake-like structures formed in the main framework were identified in Ni-containing N–Ni (Fig. S1b†) and N–CoNi (Fig. 2b). The N-free trimetallic CoNiFe (Fig. 2d) catalyst synthesized in an aqueous solution exhibited a uniform particle morphology in which particle linkages can be observed. On the other hand, the catalysts synthesized in the presence of $FeCl_3$ and EA showed a highly assembled plate-like structure (Fig. S1c†). In contrast to N–Fe, N–NiFe, and N–CoFe, relatively thin nanosheets were formed throughout the trimetallic N–CoNiFe (Fig. 2e and f). The structure of LDHs with a thin plate-like structure increases the specific surface area of the material and the active catalyst sites improves electrolyte diffusion, and accelerates charge transfer to remove the gas produced rapidly during the catalytic reaction, ultimately leading to high OER catalytic activity.

In Fig. 3, the XRD patterns of N–NiFe, N–CoNi, N–CoFe, CoNiFe, and N–CoNiFe were analyzed to identify the phase constitution of as-prepared catalysts. The XRD peaks at 11.1°, 22.4°, 33.5°, and 59.8° 2θ were assigned to the (003), (006), (012), and (110) planes of NiFe LDH (Fig. 3b), respectively. The relative peak position and intensity are well-known characteristics for correctly identifying N–CoNiFe LDHs with a hydrotalcite-like structure (Fig. 3a).[34] Fig. 3d showed sharp XRD peaks of N–CoNi, revealing the formation of crystalline $Co(OH)_2$ and $Ni(OH)_2$ structures. On the other hand, the XRD patterns of N-free CoNiFe (Fig. 3c) and N–CoFe (Fig. 3e) showed relatively poor signal-to-noise ratios and very broad peaks due to the low

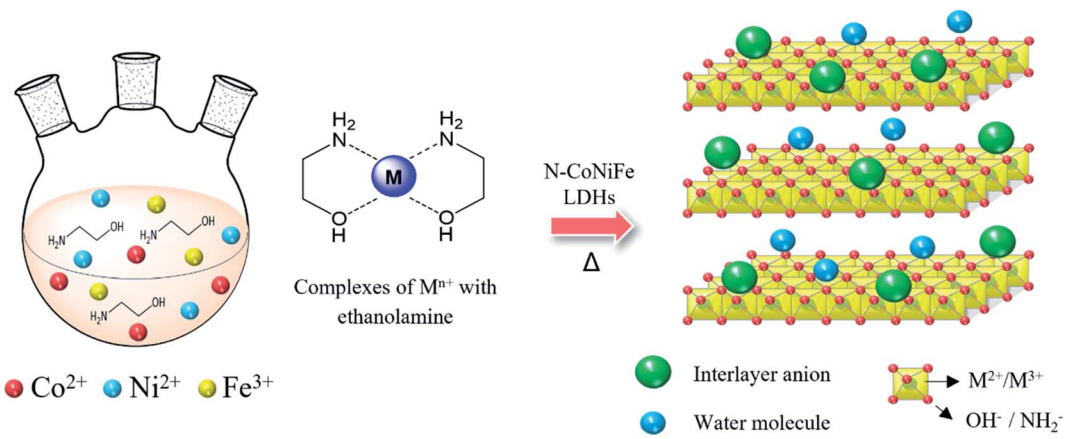

Fig. 1 Schematic diagram of the preparation of N-incorporated CoNiFe LDHs.

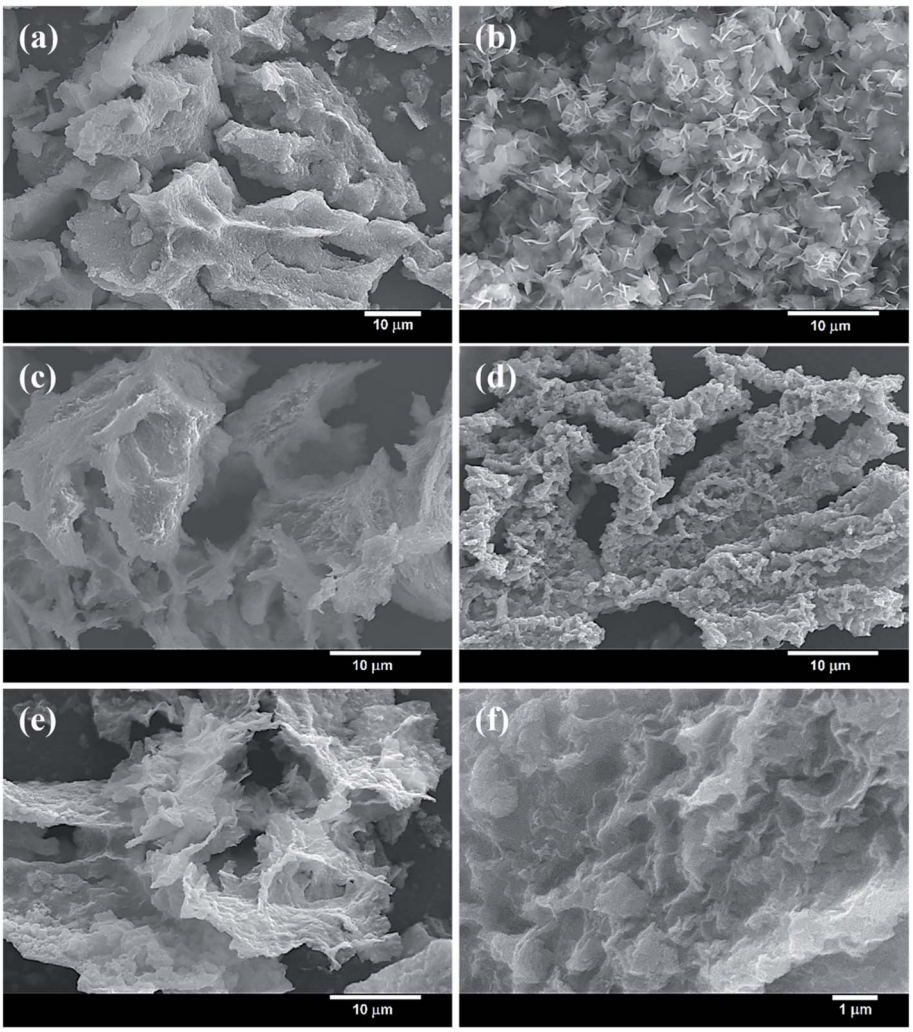

Fig. 2 SEM images of (a) N–NiFe, (b) N–CoNi, (c) N–CoFe, (d) CoNiFe, and (e and f) N–CoNiFe LDHs.

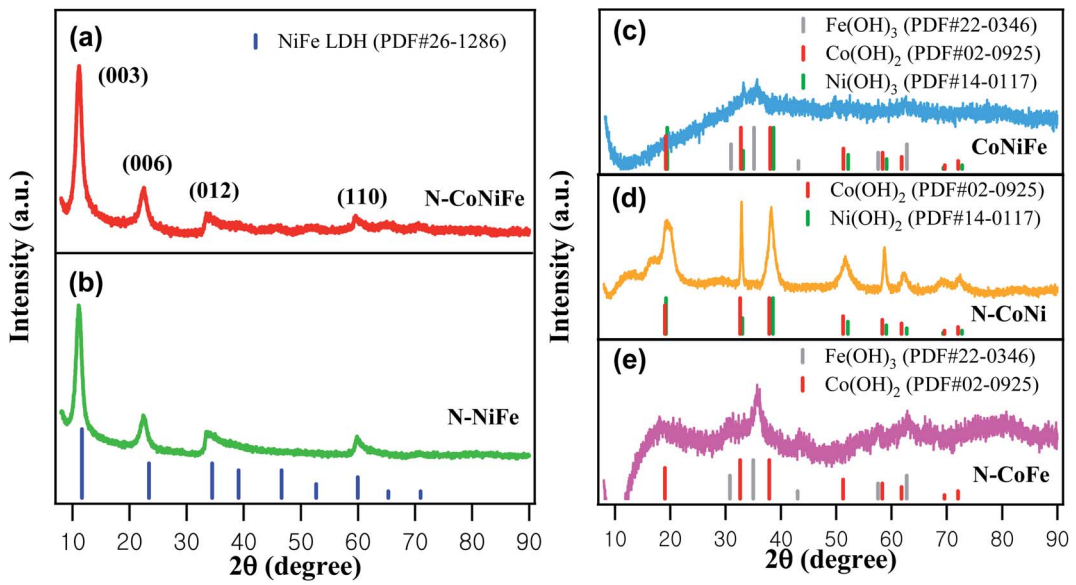

Fig. 3 XRD patterns of (a) N–CoNiFe LDH, (b) N–NiFe, (c) CoNiFe, (d) N–CoNi, and (e) N–CoFe.

crystallinity. These results indicate that EA plays an important role as a ligand in forming metallic LDH structures. Moreover, the XRD peaks of N–CoFe and CoNiFe showed the same 2θ values as that of N–Fe (Fig. S2a†), suggesting poor precipitation of Co^{2+} and Ni^{2+} without EA compared to Fe^{3+} species.

TEM (Fig. 4) revealed the more detailed morphology and structure of the as-synthesized N–CoNiFe LDHs. The porous crystalline nanosheet displays lattice fringes with the interplanar spacing of 0.24 and 0.23 nm (inset in Fig. 4a), which are related to the interplanar spacing of the (012) crystal plane of N–CoNiFe LDHs phase (Fig. 3). The energy-dispersive spectroscopy (EDS) mapping of N–CoNiFe LDHs (Fig. 4b) revealed the presence and uniform distribution of Co, Ni, Fe, and N, suggesting that nitrogen had been incorporated successfully into the CoNiFe LDHs nanostructure. SEM-EDS (Fig. S3a†) confirmed that N–CoNiFe consists of the above elements with a Co, Ni, Fe, N, and O atomic% of 9.81%, 15.99%, 7.50%, 4.63%, and 62.06%, respectively.

XPS revealed the surface elemental composition, chemical nature, and valence state of the as-prepared trimetallic N–CoNiFe. XPS of monometallic catalysts (N–Co, N–Ni, and N–Fe) were also performed to determine the relationship between structural features. Fig. S4† shows typical XPS survey scans of N–CoNiFe LDHs, which indicate the presence of C 1s, N 1s, O 1s, Co 2p, Ni 2p, and Fe 2p, showing that nitrogen had been incorporated successfully into the trimetallic CoNiFe system. The high-resolution of C 1s spectrum of N–CoNiFe shown in Fig. 5a could be divided into four different peaks with binding energies of 284.2 eV, 285.0 eV, 286.4 eV, and 288.1 eV corresponding to sp^2 hybridized C–C, sp^2 bonded with nitrogen C–N, hydroxy C–O,[35] and carboxyl C=O,[36] respectively. Fig. 5b presents the high-resolution XPS spectrum of N 1s, showing the formation of four peaks centered at 397.8 eV for cyanide CN,[37] 398.5 eV for pyridinic N, 399.0 eV for metal–nitrogen ($M–N_x$) bonding, and 400.0 eV for pyrrolic N.[38,39] The presence of $M–N_x$ species with a peak area of 34.6% indicates the bonding

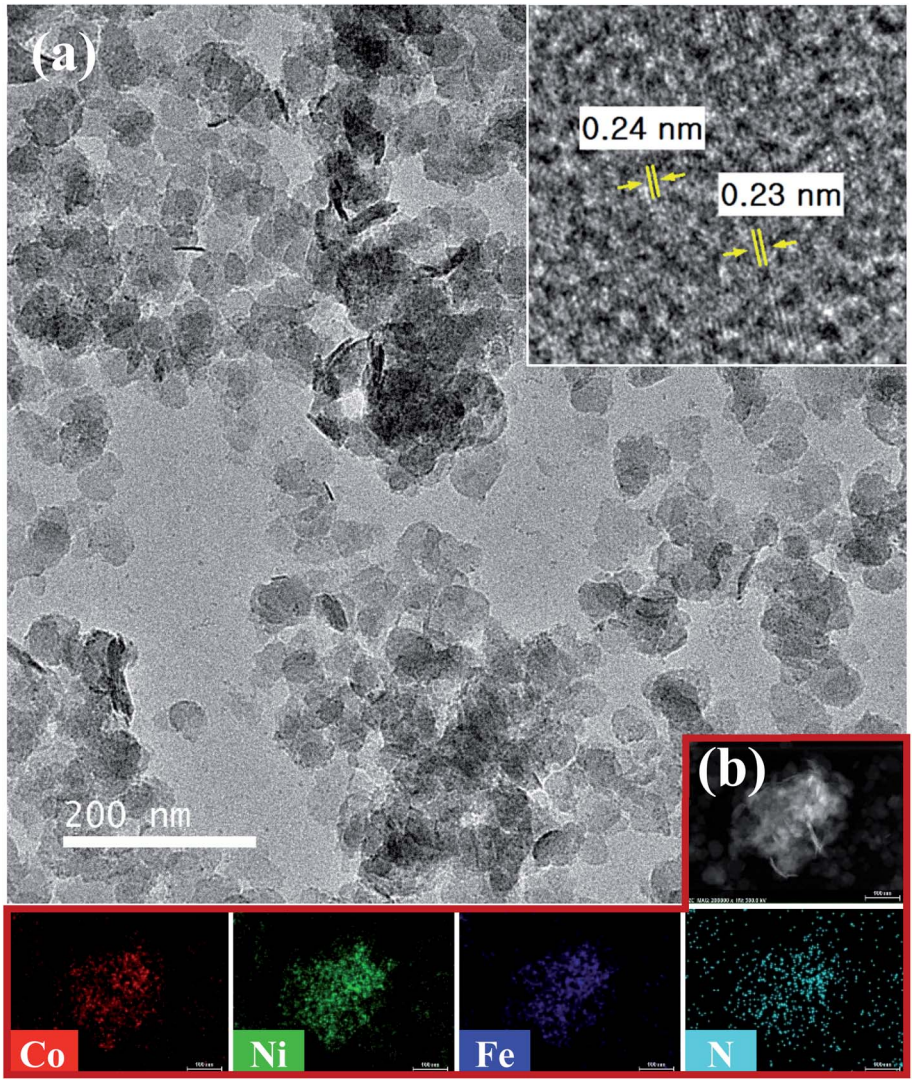

Fig. 4 (a) TEM and (b) TEM-EDS elemental mapping (scale bar: 100 nm) images of N–CoNiFe. Inset: HRTEM image of N–CoNiFe LDHs.

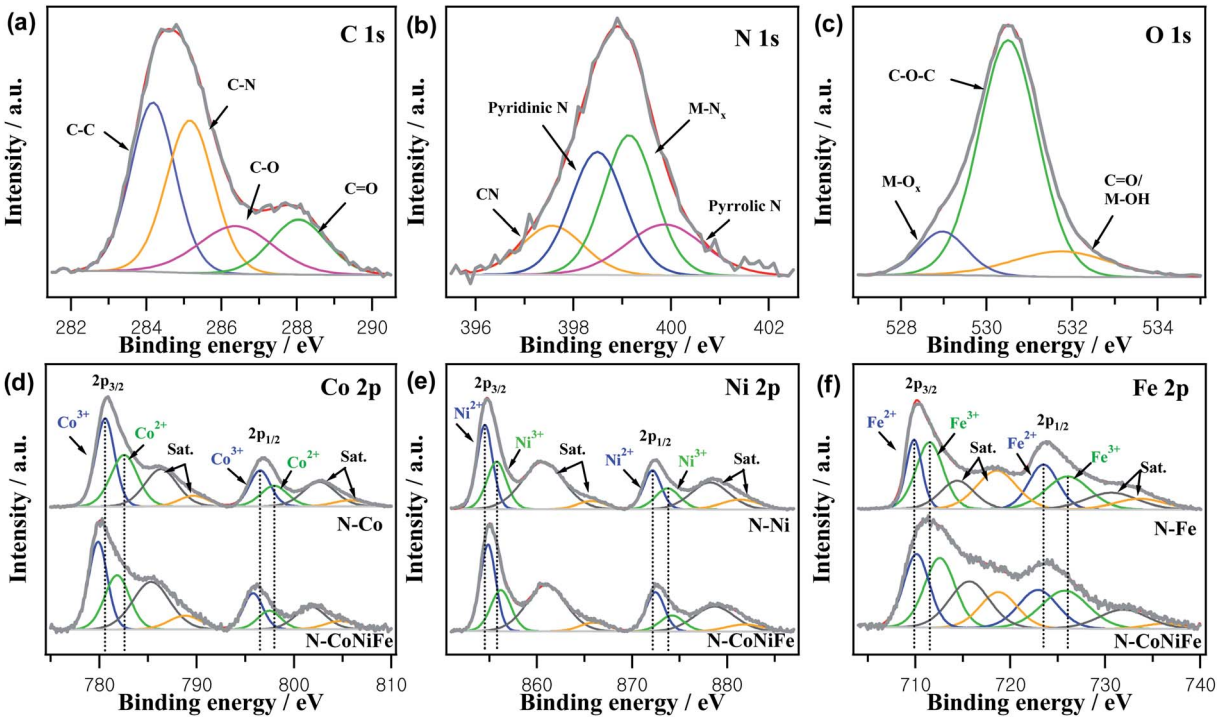

Fig. 5 XPS analysis of (a) C 1s, (b) N 1s, and (c) O 1s of N–CoNiFe LDHs. Deconvoluted XPS spectra of (d) Co 2p, (e) Ni 2p, and (f) Fe 2p of N–Co, N–Ni, N–Fe, and N–CoNiFe LDHs catalysts, respectively.

between the metal atoms and amino group *via* a coordination interaction. The O 1s peak of N–CoNiFe, located at approximately 530.9 eV was fitted to metal–oxygen (M–O$_x$) bonding, C–O–C, and C=O/M–OH[40] (Fig. 5c).

The XPS spectra of Co 2p (Fig. 5d) could be deconvoluted into two spin–orbit doublets of Co^{3+} and Co^{2+}. The major peaks of N–CoNiFe at 780.1 eV for Co 2p$_{3/2}$ and 796.0 eV for Co 2p$_{1/2}$ could be split into two distinct peaks of Co^{3+} (assigned to the 779.9 eV peak in Co 2p$_{3/2}$ and 795.8 eV peak in Co 2p$_{1/2}$) and Co^{2+} (corresponding to the 781.8 eV peak in Co 2p$_{3/2}$ and 797.5 eV peak in Co 2p$_{1/2}$). The shake-up satellite peaks were observed at 785.1 eV and 801.9 eV, which is typical for cobalt oxide.[21,26] Regarding N–CoNiFe, the deconvolution of Co 2p$_{3/2}$ and Co 2p$_{1/2}$ exhibited no significant shift compared to N–Co, showing that the other metals (Ni and Fe) did not influence the oxidation state of the Co atom. Fig. 5e represents the high-resolution spectra of the Ni 2p, comprising two spin–orbit doublets characteristic of two satellite peaks and Ni^{2+} and Ni^{3+}. Two main peaks of N–CoNiFe observed at 855.0 eV (Ni^{2+} at 854.9 eV and Ni^{3+} at 856.2 eV) and 872.6 eV (Ni^{2+} at 872.5 eV and Ni^{3+} at 874.2 eV) were attached to Ni 2p$_{3/2}$ and Ni 2p$_{1/2}$ orbits, and two satellite peaks at 861.0 eV and 879.0 eV.[21,41] For the Fe 2p XPS spectra in Fig. 5f, two peaks at 711.7 eV and 723.7 eV were assigned to Fe 2p$_{3/2}$ and Fe 2p$_{1/2}$, respectively. The Fe^{2+} peaks at 710.1 eV and Fe^{3+} at 712.6 eV were observed in the Fe 2p$_{3/2}$ region, along with Fe^{2+} and Fe^{3+} peaks at 722.9 eV and 725.7 eV, respectively, in the Fe 2p$_{1/2}$ region.[42] Compared to the deconvoluted Ni 2p and Fe 2p of monometallic N–Ni and N–Fe, the peaks of N–CoNiFe were shifted ~0.4 eV to a higher binding energy for Ni 2p and ~1.2 eV for Fe 2p, showing a change in the chemical state of Ni and Fe due to the synergistic effect between the different metal sites after the co-precipitation process. XPS deconvolution indicated the successful fabrication of N–CoNiFe LDH in this work. Compared to Co 2p, the Ni 2p and Fe 2p binding energy of N–CoNiFe shifts positively to 0.4 eV and 1.1 eV, respectively, indicating an intimate interaction between Ni and Fe and modification of the electronic structure by Ni, Fe, or Fe/Ni incorporation.[43,44] The high-valence species enrichment can enhance the electro-oxidation reactions,[43] which helps improve the OER performance.

Electrocatalytic performance

The electrochemical performance of the as-prepared electrocatalysts toward the OER was studied in a three-electrode system using a 1 M KOH electrolyte. A series of CoNiFe catalysts prepared with different EA concentrations were investigated to examine the effects of EA on its OER activity in the co-precipitation of the trimetallic system. As shown in Fig. S5a,† the LSV curves showed inferior OER activity of CoNiFe without using EA as a ligand and a stabilizing agent. N–CoNiFe was co-precipitated with a large amount of N/O doping compared to the CoNiFe counterpart because of the strong complexing with EA. The ligand acts as both an activator and deactivator of the catalytic system, depending on its concentration.[45,46] Thus, the ligand concentration was kept at a minimum to control the formation of metal complexes. The best OER catalyst was determined using 2 mL of EA at the lowest overpotential and highest current density compared to the other concentrations. The metal concentration was optimized systematically to

achieve the best synergistic effect between the metal sites (Fig. S5b†). An appropriate ratio of $[Co^{2+}]:[Ni^{2+}]:[Fe^{3+}] = 1:2:1$ was established, which corresponds to 15 mM, 30 mM, and 15 mM of the Co^{2+}, Ni^{2+}, and Fe^{3+} solutions, respectively. An irreversible anodic peak was observed at 1.4 V, which was assigned to the oxidation of Ni from the low valence states (Ni^0 or Ni^{2+}) to high valence states (Ni^{3+} or Ni^{4+}).[47,48] The Ni oxidation peak was not found in the CoNiFe catalyst because of poor precipitation in the absence of EA during the synthesis process. In particular, while the oxidation peak at 1.30–1.45 V (*vs.* RHE) was shifted negatively as the Co^{2+} concentration increased, the opposite phenomenon was observed with a change in the Fe^{3+} concentration. Interestingly, the overpotential of N–CoNiFe was influenced relatively weakly by the amount of Co^{2+}, as shown in Fig. S5b,† indicating that the ligand acetate ($-OOCCH_3$) in the cobalt precursor shows stronger binding to the center metal than EA because of the delocalized electrons between the two oxygen atoms, which is stable towards EA. XPS also demonstrated that Co is in a stable oxidation state after co-precipitation.

Fig. 6 shows the OER LSV curves for as-prepared catalysts and commercial Ir/C obtained in 1.0 M KOH at a scan rate of 10 mV s^{-1}. The overpotential required to drive 10 mA cm^{-2} corresponds to the 10% efficiency solar water-splitting units that are generally presented as a vital parameter to evaluate the OER performance of a catalyst. The trimetallic N–CoNiFe LDHs displayed an overpotential (η) of 318 mV at 10 mA cm^{-2}, which is lower than those of bimetallic N–NiFe (346 mV), N–CoNi (421 mV), N–CoFe (391 mV), CoNiFe (492 mV), and commercial Ir/C (358 mV) (Fig. 6a and c). The current density of N–CoNiFe at $\eta =$ 400 mV was 61.3 mA cm^{-2}, which was 2.5-, 9.3-, 5.1-, 41- and 3.3-fold higher than those of N–NiFe, N–CoNi, N–CoFe, CoNiFe and Ir/C, respectively (Fig. 6d). The Tafel plots extracted from the polarization curves were also analyzed to obtain more information on the OER kinetics of the catalyst. A relatively low Tafel slope is preferable because it reveals more advantageous kinetics and higher catalytic activity. As shown in Fig. 6b, the Tafel slope of N–CoNiFe was 72.2 mV dec^{-1}, which was lower than their catalyst counterparts: N–NiFe (84.9 mV dec^{-1}); N–CoNi (115.6 mV dec^{-1}); N–CoFe (83.5 mV dec^{-1}); CoNiFe (105.2 mV dec^{-1}); and Ir/C (74.1 mV dec^{-1}).

The high electrocatalytic performance of N–CoNiFe for the OER was investigated by measuring the double-layer capacitance (C_{dl}) to estimate the electrochemically active surface area (ECSA). The C_{dl} value was determined by cyclic voltammetry at various scan rates (Fig. S6†) and calculated by plotting $\Delta j = j_{anodic} - j_{cathodic}$ at 1.0 V (*vs.* RHE) as a function of the scan rate. The ECSA (cm^2) value was determined using the following equation:[49]

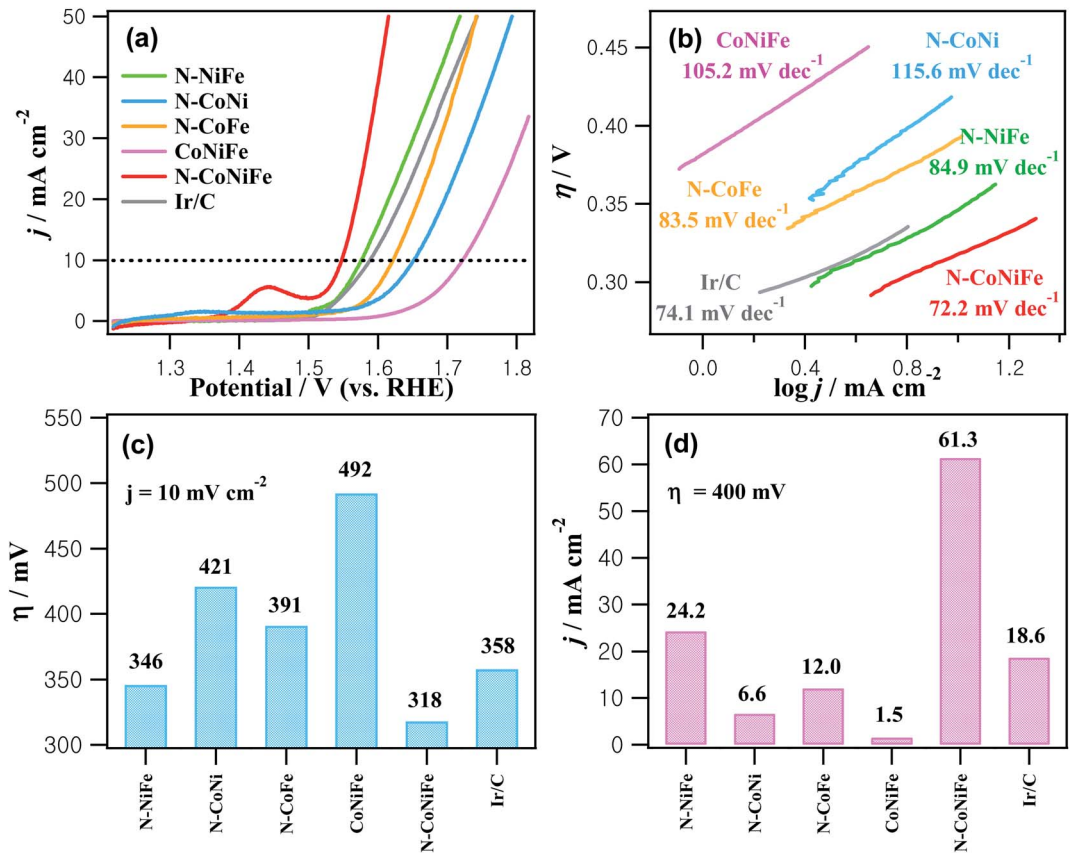

Fig. 6 (a) LSV curves recorded in an O_2-saturated 1.0 M KOH at a scan rate of 10 mV s^{-1} (rotational speed of 1600 rpm). (b) Tafel plots. (c) Comparative overpotential at 10 mV cm^{-2}. (d) Current densities at $\eta = 400$ mV. The electrodes used in the electrocatalytic OER: N–NiFe; N–CoNi; N–CoFe; CoNiFe; N–CoNiFe; and Ir/C.

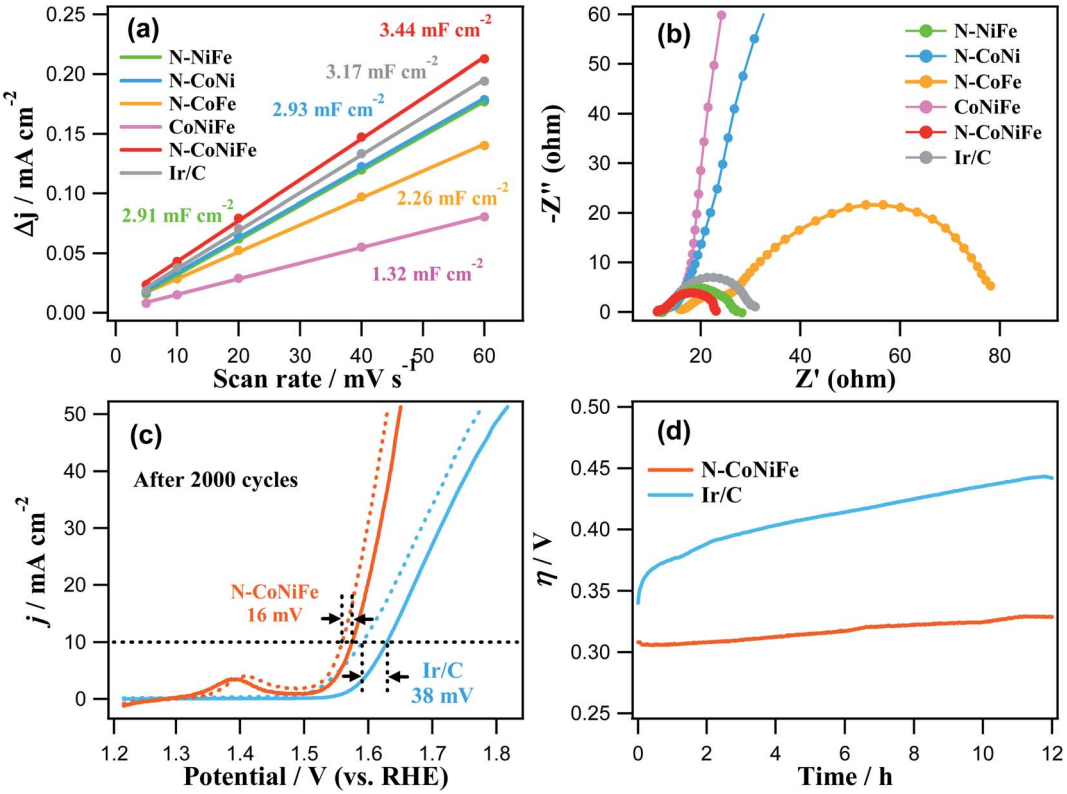

Fig. 7 (a) Plots of the capacitive current density (Δj in 1.0 V) as a function of the scan rate shown in Fig. S6.† (b) EIS plots of N–NiFe, N–CoNi, N–CoFe, CoNiFe, N–CoNiFe, and Ir/C. (c) Stability test of the N–CoNiFe and Ir/C for the OER before and after 2000 cycles on the GC electrode in a 1.0 M KOH solution at a scan rate of 10 mV s^{-1}. (d) Chronopotentiometric response of N–CoNiFe and Ir/C at the current density of 10 mA cm^{-2}.

$$\mathrm{ECSA} = \frac{C_{\mathrm{dl}}}{C_{\mathrm{s}}} = \frac{i_{\mathrm{c}}}{\nu C_{\mathrm{s}}}$$

where C_s, i_c, and ν are the specific capacitance (27 μF cm^{-2}), charging current, and scan rate, respectively.

Fig. 7a and Table 1 show that the trimetallic N–CoNiFe LDHs catalyst had the highest C_{dl} value (3.44 mF cm^{-2}) and ECSA (127.4 cm^2) compared to bimetallic N–NiFe, N–CoNi, N–CoFe, and CoNiFe. These results show that the LDH-formed N–CoNiFe catalyst can absorb and desorb water molecules and gas products, suggesting that the N–CoNiFe LDHs sample can provide more active sites than the other samples, resulting in superior OER activity. The BET specific surface area and pore distribution were determined to characterize the surface area of CoNiFe and N–CoNiFe. In the case of N–CoNiFe, the BET specific surface area in Fig. S7† was 161.4 m^2 g^{-1}, which was significantly larger than that of the N-free CoNiFe catalyst. The pore size distribution of N–CoNiFe (0.665 cm^3 g^{-1}) was calculated by Barrett–Joyner–Halenda method revealing a relatively wider distribution compared with CoNiFe. The LDH structure of N–CoNiFe exhibiting mesoporosity (average pore diameter, $d \approx$ 12.8 nm) is beneficial in terms of O_2 generation because of the improved active site densities. EIS was carried out at η = 337.4 mV to determine the different charge transfer rates during the OER of the catalysts. As shown in Fig. 7b, a relatively higher charge transfer resistance (R_{ct}) was observed in N–CoNi and N-free CoNiFe, increasing the potential barrier and reaction kinetics of the catalyst. The low crystallinity of N-free CoNiFe synthesized in the absence of EA leads to higher R_{ct} curves with increased resistance to charge transfer (lower rate constant). On

Table 1 Comparison of the electrocatalytic OER characteristics of various samples

Samples	η (mV) (at 10 mA cm^{-2})	j (mA cm^{-2}) (at η = 400 mV)	Tafel slope (mV dec^{-1})	C_{dl} (mF cm^{-2})	ECSA (cm^2)
N–NiFe	346	24.2	84.9	2.91	107.8
N–CoNi	421	6.6	115.6	2.93	108.5
N–CoFe	391	12.0	83.5	2.26	83.7
CoNiFe	492	1.5	105.2	1.32	48.9
N–CoNiFe	318	61.3	72.2	3.44	127.4
Ir/C	358	18.6	74.1	3.17	117.4

the other hand, the overall resistance of N–CoNiFe LDHs had the lowest R_{ct} value among the catalysts, suggesting that the N–CoNiFe LDHs have favorable charge transfer kinetics and mass transfer in the OER process. Indeed, the observed R_{ct} values were similar to the trend of an OER performance resulting in the reduced R_{ct} value and more active OER.

In addition to the catalytic performance, N–CoNiFe also showed high stability and durability in the OER process. As shown in Fig. 7c, the overpotential of N–CoNiFe at 10 mA cm^{-2} was positively shifted 16 mV after 2000 CV cycles, which is smaller than commercial Ir/C (38 mV). These results suggest that the N–CoNiFe catalyst has high catalytic activity and good stability in the OER after a long-term cycle. The SEM and SEM-EDS results showed that the surface morphology and composition of the N–CoNiFe catalyst remained almost unchanged before and after the stability cycling (Fig. S3a and S8†). Moreover, the N–CoNiFe LDHs remained stable over the 12 h OER process at the current density of 10 mA cm^{-2}, whereas the η values of Ir/C increased rapidly in just a few hours (Fig. 7d). Table S1† shows a list of several reported CoNiFe catalysts with various structural features. The intrinsically high activity of N–CoNiFe was attributed to the following aspects. First, the synergistic effects of metal species play a vital role in enhancing the electronic conductivity and altering the adsorption energies for the reaction intermediate. Second, the improving specific surface area and active sites in the porous structure of nanosheets provided by nitrogen doping allow rapid electrolyte penetration and charge/ion transfer, as well the more accessible release of gases produced during water electrolysis.

Conclusions

Nitrogen-incorporated trimetallic CoNiFe LDHs catalysts were prepared using a rapid, facile, controllable, and economical method. The N–CoNiFe LDHs showed good electrocatalytic efficiency and high stability for the OER, with a low overpotential of 318 mV at 10 mA cm^{-2}, and a low Tafel slope of 72.2 mV dec^{-1} in a 1.0 M KOH solution. In addition, the catalyst shows high durability in the OER process with little change in the overpotential (*ca.* 16.0 mV) at 10 mA cm^{-2} after 2000 cycles, which was smaller than commercial Ir/C (38.0 mV). Thus, the results show that the N–CoNiFe LDH is a promising nanomaterial in terms of high-performance and cost-effective catalyst for the OER. Moreover, the method for fabricating N-incorporated trimetallic LDHs catalyst is a practical approach to achieve large-scale production.

Conflicts of interest

There are no conflicts to declare.

Acknowledgements

This work was supported by the Dongil Culture and Scholarship Foundation (2021), and the National Research Foundation of Korea (NRF) grant funded by the Korea Government (MSIT) (No. 2019R1F1A1049614 and No. 2021R1F1A1063825).

References

1 S. E. Hosseini and M. A. Wahid, Hydrogen production from renewable and sustainable energy resources: promising green energy carrier for clean development, *Renewable Sustainable Energy Rev.*, 2016, **57**, 850–866.
2 F. Dawood, M. Anda and G. M. Shafiullah, Hydrogen production for energy: an overview, *Int. J. Hydrogen Energy*, 2020, **45**, 3847–3869.
3 O. Schmidt, A. Gambhir, I. Staffell, A. Hawkes, J. Nelson and S. Few, Future cost and performance of water electrolysis: an expert elicitation study, *Int. J. Hydrogen Energy*, 2017, **42**, 30470–30492.
4 X. Li, X. Hao, A. Abudula and G. Guan, Nanostructured catalysts for electrochemical water splitting: current state and prospects, *J. Mater. Chem. A*, 2016, **4**, 11973–12000.
5 A. T. N. Nguyen and J. H. Shim, Facile one-step synthesis of Ir-Pd bimetallic alloy networks as efficient bifunctional catalysts for oxygen reduction and oxygen evolution reactions, *J. Electroanal. Chem.*, 2018, **827**, 120–127.
6 Y. Kweon, S. Noh and J. H. Shim, Low content Ru-incorporated Pd nanowires for bifunctional electrocatalysis, *RSC Adv.*, 2021, **11**, 28775–28784.
7 J.-W. Zhang, H. Zhang, T.-Z. Ren, Z.-Y. Yuan and T. J. Bandosz, FeNi doped porous carbon as an efficient catalyst for oxygen evolution reaction, *Front. Chem. Sci. Eng.*, 2021, **15**, 279–287.
8 L. Yang, L. Chen, D. Yang, X. Yu, H. Xue and L. Feng, NiMn layered double hydroxide nanosheets/$NiCo_2O_4$ nanowires with surface rich high valence state metal oxide as an efficient electrocatalyst for oxygen evolution reaction, *J. Power Sources*, 2018, **392**, 23–32.
9 W. Li, D. Xiong, X. Gao and L. Liu, The oxygen evolution reaction enabled by transition metal phosphide and chalcogenide pre-catalysts with dynamic changes, *Chem. Commun.*, 2019, **55**, 8744–8763.
10 Y. Du, S. Khan, X. Zhang, G. Yu, R. Liu, B. Zheng, R. Nadimicherla, D. Wu and R. Fu, In situ preparation of porous carbon nanosheets loaded with metal chalcogenides for a superior oxygen evolution reaction, *Carbon*, 2019, **149**, 144–151.
11 J.-Y. Xue, C. Li, F.-L. Li, H.-W. Gu, P. Braunstein and J.-P. Lang, Recent advances in pristine tri-metallic metal–organic frameworks toward the oxygen evolution reaction, *Nanoscale*, 2020, **12**, 4816–4825.
12 L. Kuai, J. Geng, C. Chen, E. Kan, Y. Liu, Q. Wang and B. Geng, A reliable aerosol-spray-assisted approach to produce and optimize amorphous metal oxide catalysts for electrochemical water splitting, *Angew. Chem., Int. Ed. Engl.*, 2014, **53**, 7547–7551.
13 C. Yang, W.-J. Cai, B.-B. Yu, H. Qiu, M.-L. Li, L.-W. Zhu, Z. Yan, L. Hou and Y.-Y. Wang, Performance enhancement of oxygen evolution reaction through incorporating bimetallic electrocatalysts in two-dimensional metal–organic frameworks, *Catal. Sci. Technol.*, 2020, **10**, 3897–3903.

14 S. Jo, S. Noh, K.-R. Wee and J. H. Shim, Structural Features of Porous CoFe Nanocubes and Their Performance for Oxygen-involving Energy Electrocatalysis, *ChemElectroChem*, 2020, **7**, 3725–3732.

15 R. D. L. Smith, M. S. Prévot, R. D. Fagan, S. Trudel and C. P. Berlinguette, Water oxidation catalysis: electrocatalytic response to metal stoichiometry in amorphous metal oxide films containing iron, cobalt, and nickel, *J. Am. Chem. Soc.*, 2013, **135**, 11580–11586.

16 Z. Cai, X. Bu, P. Wang, J. C. Ho, J. Yang and X. Wang, Recent advances in layered double hydroxide electrocatalysts for the oxygen evolution reaction, *J. Mater. Chem. A*, 2019, **7**, 5069–5089.

17 R. Chen, S.-F. Hung, D. Zhou, J. Gao, C. Yang, H. Tao, H. B. Yang, L. Zhang, L. Zhang, Q. Xiong, H. M. Chen and B. Liu, Layered structure causes bulk NiFe layered double hydroxide unstable in alkaline oxygen evolution reaction, *Adv. Mater.*, 2019, **31**, 1903909.

18 J. Jiang, A. Zhang, L. Li and L. Ai, Nickel–cobalt layered double hydroxide nanosheets as high-performance electrocatalyst for oxygen evolution reaction, *J. Power Sources*, 2015, **278**, 445–451.

19 F. Yang, K. Sliozberg, I. Sinev, H. Antoni, A. Bähr, K. Ollegott, W. Xia, J. Masa, W. Grünert, B. R. Cuenya, W. Schuhmann and M. Muhler, Synergistic effect of cobalt and iron in layered double hydroxide catalysts for the oxygen evolution reaction, *ChemSusChem*, 2017, **10**, 156–165.

20 K. Yue, J. Liu, Y. Zhu, C. Xia, P. Wang, J. Zhang, Y. Kong, X. Wang, Y. Yan and B. Y. Xia, In situ ion-exchange preparation and topological transformation of trimetal–organic frameworks for efficient electrocatalytic water oxidation, *Energy Environ. Sci.*, 2021, **14**, 6546–6553.

21 F. Li, Z. Sun, H. Jiang, Z. Ma, Q. Wang and F. Qu, Ion-exchange synthesis of ternary FeCoNi-layered double hydroxide nanocage toward enhanced oxygen evolution reaction and supercapacitor, *Energy Fuels*, 2020, **34**, 11628–11636.

22 Y. Yang, L. Dang, M. J. Shearer, H. Sheng, W. Li, J. Chen, P. Xiao, Y. Zhang, R. J. Hamers and S. Jin, Highly active trimetallic NiFeCr layered double hydroxide electrocatalysts for oxygen evolution reaction, *Adv. Energy Mater.*, 2018, **8**, 1703189.

23 J.-T. Ren, Y.-S. Wang, L. Chen, L.-J. Gao, W.-W. Tian and Z.-Y. Yuan, Binary FeNi phosphides dispersed on N,P-doped carbon nanosheets for highly efficient overall water splitting and rechargeable Zn-air batteries, *Chem. Eng. J.*, 2020, **389**, 124408.

24 X.-W. Lv, W.-S. Xu, W.-W. Tian, H.-Y. Wang and Z.-Y. Yuan, Activity promotion of core and shell in multifunctional core–shell Co_2P@NC electrocatalyst by secondary metal doping for water electrolysis and Zn-air batteries, *Small*, 2021, **17**, 2101856.

25 M. Al-Mamun, Z. Zhu, H. Yin, X. Su, H. Zhang, P. Liu, H. Yang, D. Wang, Z. Tang, Y. Wang and H. Zhao, The surface sulfur doping induced enhanced performance of cobalt catalysts in oxygen evolution reactions, *Chem. Commun.*, 2016, **52**, 9450–9453.

26 S. V. S. Mers, V. Maruthapandian and V. Ganesh, Highly efficient bifunctional electrocatalyst using structurally architectured N-doped cobalt oxide, *ChemistrySelect*, 2018, **3**, 8752–8762.

27 L.-M. Cao, J.-W. Wang, D.-C. Zhong and T.-B. Lu, Template-directed synthesis of sulphur doped NiCoFe layered double hydroxide porous nanosheets with enhanced electrocatalytic activity for the oxygen evolution reaction, *J. Mater. Chem. A*, 2018, **6**, 3224–3230.

28 J.-J. Duan, R.-L. Zhang, J.-J. Feng, L. Zhang, Q.-L. Zhang and A.-J. Wang, Facile synthesis of nanoflower-like phosphorus-doped Ni_3S_2/$CoFe_2O_4$ arrays on nickel foam as a superior electrocatalyst for efficient oxygen evolution reaction, *J. Colloid Interface Sci.*, 2021, **581**, 774–782.

29 I.-K. Ahn, S.-Y. Lee, H. G. Kim, G.-B. Lee, J.-H. Lee, M. Kim and Y.-C. Joo, Electrochemical oxidation of boron-doped nickel–iron layered double hydroxide for facile charge transfer in oxygen evolution electrocatalysts, *RSC Adv.*, 2021, **11**, 8198–8206.

30 D. Zhou, Z. Cai, X. Lei, W. Tian, Y. Bi, Y. Ji, N. Han, T. Gao, Q. Zhang, Y. Kuang, J. Pan, X. Sun and X. Duan, NiCoFe-layered double hydroxides/N-doped graphene oxide array colloid composite as an efficient bifunctional catalyst for oxygen electrocatalytic reactions, *Adv. Energy Mater.*, 2017, 1701905.

31 M. Amjad, S. H. Sumrra, M. S. Akram and Z. H. Chohan, Metal-based ethanolamine-derived compounds: a note on their synthesis, characterization and bioactivity, *J. Enzyme Inhib. Med. Chem.*, 2016, **31**, 88–97.

32 S. Sahu, U. K. Sahu and R. K. Patel, Synthesis of thorium–ethanolamine nanocomposite by the co-precipitation method and its application for Cr(vi) removal, *New J. Chem.*, 2018, **42**, 5556–5569.

33 M. S. Masoud, A. E. Ali, H. M. Ahmed and E. A. Mohamed, Spectral studies and thermal analysis of new vanadium complexes of ethanolamine and related compounds, *J. Mol. Struct.*, 2013, **1050**, 43–52.

34 C. Dong, L. Han, C. Zhang and Z. Zhang, Scalable dealloying route to mesoporous ternary CoNiFe layered double hydroxides for efficient oxygen evolution, *ACS Sustainable Chem. Eng.*, 2018, **6**, 16096–16104.

35 T. Feng, Q. Zeng, S. Lu, M. Yang, S. Tao, Y. Chen, Y. Zhao and B. Yang, Morphological and interfacial engineering of cobalt-based electrocatalysts by carbon dots for enhanced water splitting, *ACS Sustainable Chem. Eng.*, 2019, **7**, 7047–7057.

36 C. L. Chiang and J. M. Yang, in *Novel Fire Retardant Polymers and Composite Materials*, ed. D.-Y. Wang, Woodhead Publishing, 2017, pp. 295–312.

37 A. Cano, J. Rodríguez-Hernández, A. Shchukarev and E. Reguera, Intercalation of pyrazine in layered copper nitroprusside: synthesis, crystal structure and XPS study, *J. Solid State Chem.*, 2019, **273**, 1–10.

38 T.-N. Tran, H.-Y. Lee, J.-D. Park, T.-H. Kang, B.-J. Lee and J.-S. Yu, Synergistic CoN-decorated Pt catalyst on two-dimensional porous Co–N-doped carbon nanosheet for

enhanced oxygen reduction activity and durability, *ACS Appl. Energy Mater.*, 2020, **3**, 6310–6322.

39 H. Peng, Z. Mo, S. Liao, H. Liang, L. Yang, F. Luo, H. Song, Y. Zhong and B. Zhang, High performance Fe- and N-doped carbon catalyst with graphene structure for oxygen reduction, *Sci. Rep.*, 2013, **3**, 1765.

40 J.-C. Dupin, D. Gonbeau, P. Vinatier and A. Levasseur, Systematic XPS studies of metal oxides, hydroxides and peroxides, *Phys. Chem. Chem. Phys.*, 2000, **2**, 1319–1324.

41 Y. Xue, Y. Wang, H. Liu, X. Yu, H. Xue and L. Feng, Electrochemical oxygen evolution reaction catalyzed by a novel nickel–cobalt-fluoride catalyst, *Chem. Commun.*, 2018, **54**, 6204–6207.

42 H. Liu, Y. Li, M. Yuan, G. Sun, Q. Liao and Y. Zhang, Solid and macroporous Fe_3C/N-C nanofibers with enhanced electromagnetic wave absorbability, *Sci. Rep.*, 2018, **8**, 16832.

43 W. Liu, J. Xie, Y. Guo, S. Lou, L. Gao and B. Tang, Sulfurization-induced edge amorphization in copper–nickel–cobalt layered double hydroxide nanosheets promoting hydrazine electrooxidation, *J. Mater. Chem. A*, 2019, **7**, 24437–24444.

44 H. Wang and S. Tao, Fabrication of a porous NiFeP/Ni electrode for highly efficient hydrazine oxidation boosted H_2 evolution, *Nanoscale Adv.*, 2021, **3**, 2280–2286.

45 K. Matyjaszewski, in *Encyclopedia of Materials: Science and Technology*, ed. K. H. J. Buschow, R. W. Cahn, M. C. Flemings, B. Ilschner, E. J. Kramer, S. Mahajan and P. Veyssière, Elsevier, Oxford, 2001, pp. 356–365.

46 Y. I. Yermakov, B. N. Kuznetsov and V. A. Zakharov, in *Studies in Surface Science and Catalysis*, ed. Elsevier, 1981, vol. 8, pp. 1–58.

47 L.-A. Stern and X. Hu, Enhanced oxygen evolution activity by NiO_x and $Ni(OH)_2$ nanoparticles, *Faraday Discuss.*, 2014, **176**, 363–379.

48 B. H. R. Suryanto, Y. Wang, R. K. Hocking, W. Adamson and C. Zhao, Overall electrochemical splitting of water at the heterogeneous interface of nickel and iron oxide, *Nat. Commun.*, 2019, **10**, 5599.

49 H. Lei, M. Chen, Z. Liang, C. Liu, W. Zhang and R. Cao, Ni_2P hollow microspheres for electrocatalytic oxygen evolution and reduction reactions, *Catal. Sci. Technol.*, 2018, **8**, 2289–2293.